Effects of short-range order on the electronic structure of disordered metallic systems

Derwyn A. Rowlands,[1] Julie B. Staunton,[2] Balazs L. Györffy,[1] Ezio Bruno,[3] and Beniamino Ginatempo[3]
[1]*H. H. Wills Physics Laboratory, University of Bristol, Bristol BS8 1TL, United Kingdom*
[2]*Department of Physics, University of Warwick, Coventry CV4 7AL, United Kingdom*
[3]*Dipartimento di Fisica, Universita di Messina Salita Sperone 31, 98166 Messina, Italy*
(Received 27 January 2005; published 1 July 2005)

For many years the Korringa-Kohn-Rostoker coherent-potential approximation (KKR-CPA) has been widely used to describe the electronic structure of disordered systems based upon a first-principles description of the crystal potential. However, as a single-site theory the KKR-CPA is unable to account for important environmental effects such as short-range order (SRO) in alloys and spin fluctuations in magnets, among others. Using the recently devised KKR-NLCPA (where NL stands for nonlocal), we show how to remedy this by presenting explicit calculations for the effects of SRO on the electronic structure of the bcc $Cu_{50}Zn_{50}$ solid solution.

DOI: 10.1103/PhysRevB.72.045101 PACS number(s): 71.15.Ap, 71.15.Mb, 71.20.Be, 71.23.−k

I. INTRODUCTION

Currently, the first-principles theory of electrons in disordered metals is based upon density functional theory (DFT) and either the Korringa-Kohn-Rostoker coherent-potential spproximation (KKR-CPA)[1–3] or its stripped down version, the linear muffin-tin orbital (LMTO)-CPA,[4] for averaging over the random configurations. This approach has been successfully applied to cases where the disorder is internal as well as external. Examples of the latter are metallic solid solutions such as $Cu_cZn_{(1-c)}$ and $Cu_cPd_{(1-c)}$ above their ordering temperatures T_0. Examples of the former are Fe or Ni above their Curie temperatures T_c, where randomness in the crystal potential seen by an electron is the consequence of disordered local moments (DLM)[5] and secondly valence fluctuating systems such as Ce.[6] Despite significant achievements,[7,8] this methodology suffers from the shortcoming of not describing correlations in the fluctuations of the crystal potential. However a generalization of the KKR-CPA theory has recently been proposed, the KKR-NLCPA (where NL stands for nonlocal),[9,10] which systematically takes into account such correlations, enabling environmental effects such as short-range order (SRO) to be taken into account. Although the full three-dimensional (3D) KKR-NLCPA formalism was given in Refs. 9 and 10, in this paper we present the first realistic 3D implementation of the theory[11] by illustrating the effects of SRO on the $Cu_{50}Zn_{50}$ system.

The physics of the above SRO plays a particularly important role near phase transitions where it is frequently a precursor for long-range order and can be said to be driving the ordering process. For example, in the ordering of the $Cu_{50}Zn_{50}$ solid solution into an intermetallic compound of $B2$ symmetry, the system lowers its free energy by having unlike neighbors more frequently than like neighbors even in the disordered state, thereby lowering the temperature T_0 where the system must finally order. Such SRO is also central to the understanding of electronic transport in general and in K-state alloys in particular.[12,13] Moreover, the formation of the moment in the DLM state of Ni (Ref. 5) and the creation of γ-like Ce atoms near the γ-α transition[6] will be materially affected by the SRO. The KKR-NLCPA method to be illustrated here will enable these important problems to be tackled in a parameter-independent and material-specific way. However, before getting on with the task, we comment briefly on efforts addressing the same problem as we do by adopting alternative strategies.

There have been several attempts to develop cluster generalizations of the single-site CPA. As with the CPA, the main construct is an effective medium so that the motion of an electron through it approximates the motion, *on the average*, of the electron in the disordered system. An early example, the molecular CPA (MCPA),[14] introduces a supercell so that the medium has the unsatisfactory attribute of broken translational symmetry. The embedded cluster method (ECM)[15,16] refers to the non-self-consistent embedding of a cluster with all the relevant disorder configurations into the CPA medium. The travelling cluster approximation (TCA)[17] based on diagrammatic methods and the cluster-CPA (C-CPA)[18,19] based on the augmented space formalism (ASF)[20,21] are, like the NLCPA, satisfactory on account of their translationally invariant, self-consistently determined effective media and herglotz analytic properties. Both the TCA and C-CPA become rapidly computationally intractable, however, and a KKR version of the latter has been applied only to model systems.[19,22] A reasonably good alternative starting point for the electronic structure of some disordered alloys is the tight-binding (TB)-LMTO method[4] combined with the CPA, which can include an approximate treatment of the charge self-consistency needed for a DFT. Mookerjee and Prasad[23] have developed a generalized ASF with correlated variables to describe SRO, which has been combined with the TB-LMTO and real-space recursion technique.[24] This approach has been used successfully to describe effects of SRO on the densities of states of several alloy systems.[25,26] Nonetheless it is desirable to develop a computationally tractable generalization of the CPA within the KKR method, the KKR-NLCPA, with fewer approximations and superiority with regards to accuracy and reliability over LMTO methods. It will also be amenable for incorporation into a full DFT description of disordered materials with SRO.[27]

This paper is organized as follows. In Sec. II we briefly summarize the idea of the KKR-NLCPA (for the full derivation, see Refs. 9 and 10), and in particular we clearly explain how to carry out the fundamental "coarse-graining" procedure for general lattices. Our aim is to show how current KKR-based computational codes can be straightforwardly adapted to include the KKR-NLCPA with its capability of dealing with disordered systems with SRO. In Sec. III we present results including SRO calculations for the $Cu_{50}Zn_{50}$ system, and we conclude in Sec. IV.

II. FORMALISM

The first step is to define the scattering path matrix $\hat{\underline{\tau}}^{ij}$ describing the motion of an electron in an effective medium, which ideally should be determined so that it would describe the average properties of an electron exactly. It is a quantity that describes the full effects of the coherent potential and is given by

$$\hat{\underline{\tau}}^{ij} = \hat{\underline{t}}\delta_{ij} + \sum_{k\neq i} \hat{\underline{t}}(\underline{G}(\mathbf{R}_{ik}) + \underline{\widehat{\delta G}}(\mathbf{R}_{ik}))\hat{\underline{\tau}}^{kj}. \quad (1)$$

Here a circumflex symbol denotes an effective medium quantity and an underscore denotes a matrix in angular momentum space. In addition to effective local t matrices $\hat{\underline{t}}$ and the usual free-space KKR structure constants $\underline{G}(\mathbf{R}_{ij})$ that account for the lattice structure, we also have effective structure constant corrections $\underline{\widehat{\delta G}}(\mathbf{R}_{ij})$ that take into account all nonlocal scattering correlations due to the disorder configurations (labelled $\hat{\underline{\alpha}}^{ij}$ in Ref. 10). Since the effective medium is translationally invariant, the matrix elements $\hat{\underline{\tau}}^{ij}$ are also given by the Brillouin zone (BZ) integral

$$\hat{\underline{\tau}}^{ij} = \frac{1}{\Omega_{BZ}}\int_{\Omega_{BZ}} d\mathbf{k}(\hat{\underline{t}}^{-1} - \underline{G}(\mathbf{k}) - \underline{\widehat{\delta G}}(\mathbf{k}))^{-1} e^{i\mathbf{k}(\mathbf{R}_i - \mathbf{R}_j)}. \quad (2)$$

Since it is not feasible to solve the problem exactly, the key idea, based upon concepts from the dynamical cluster approximation,[28,29] is to perform a consistent coarse graining in both real and reciprocal space in order to appropriately deal with $\underline{\widehat{\delta G}}(\mathbf{R}_{ij})$ and $\underline{\widehat{\delta G}}(\mathbf{k})$, respectively. The construction for carrying out this coarse graining, which must retain the translational invariance and point-group symmetry of the underlying lattice, has been given by Jarrell and Krishnamurthy[29] for a 2D square lattice in connection with a simple tight-binding model Hamiltonian. We have generalized this construction for realistic 3D body-centered cubic (bcc), face-centered cubic (fcc), and simple cubic (sc) lattices,[9–11] which we implement for the first time here.

First we summarize the construction for a general lattice. Technically, the task is to find an appropriate set of N_c real-space cluster sites $\{I,J\}$ and corresponding set of "cluster momenta" $\{\mathbf{K}_n\}$, satisfying the relation

$$\frac{1}{N_c}\sum_{\mathbf{K}_n} e^{i\mathbf{K}_n(\mathbf{R}_I - \mathbf{R}_J)} = \delta_{IJ}. \quad (3)$$

This may be accomplished as follows:

(1) Choose a real-space cluster of N_c sites that can be surrounded by a *tile* that (a) preserves the point-group symmetry of the underlying lattice and (b) can be periodically repeated to fill out all space. For $N_c=1$, the tiles are the conventional Wigner-Seitz cells surrounding each lattice point, as shown for the bcc lattice in Fig. 1(a). For $N_c>1$ there may only be solutions to the problem for particular values of N_c for any given lattice. For the bcc lattice the next allowed cluster sizes are $N_c=2$ and 16, where the tiles are

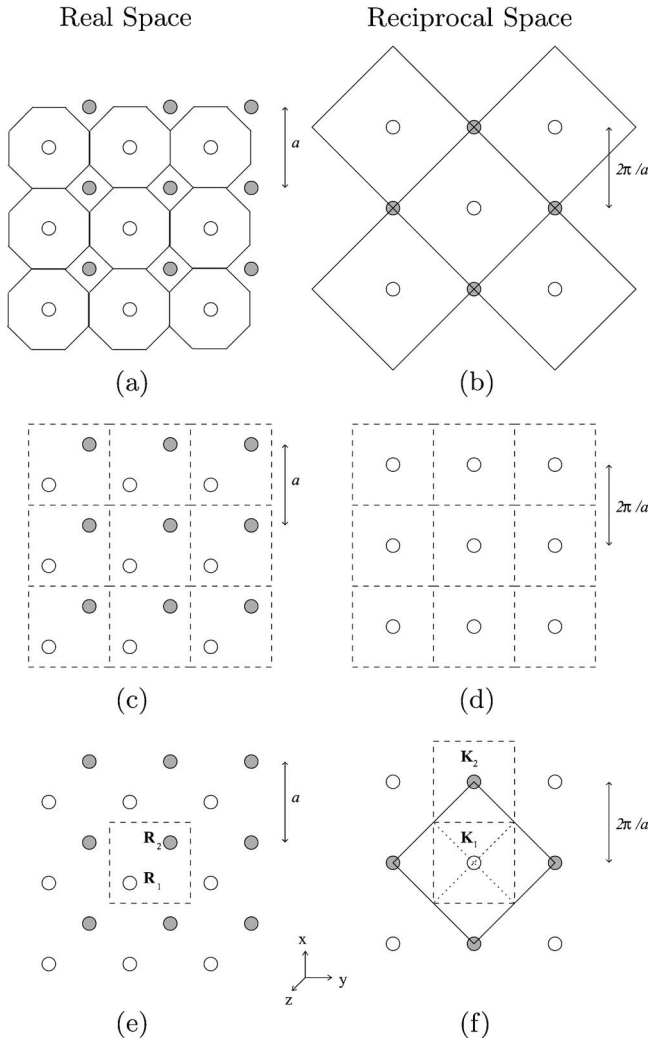

FIG. 1. Example (bcc lattice): (a) Cross section of the conventional real-space tiling with Wigner-Seitz cells. The shaded sites lie outside of the page. (b) Cross section of the conventional reciprocal-space tiling with Brillouin zones. The shaded sites lie outside of the page. (c) Cross section of the real-space tiling (dashed lines) with $N_c=2$. (d) Cross section of the reciprocal lattice points and reciprocal-space tiles (dashed lines) of the coarse-grained system. (e) Cross section of a real-space tile (dashed line) for a $N_c=2$ cluster containing the points $\mathbf{R}_1=(0,0,0)$ and $\mathbf{R}_2=(a/2,a/2,a/2)$. The shaded sites lie outside of the page. (f) Cross section of the corresponding reciprocal-space tiles (dashed lines) for the $N_c=2$ cluster, with $\mathbf{K}_1=(0,0,0)$ and $\mathbf{K}_2=(2\pi/a,0,0)$ at their centers. The shaded points lie outside of the page and the solid line denotes a cross section of the first BZ in the (k_x,k_y) plane. The BZ can be visualized as a cube with a pyramid attached to each of the six faces, and the dotted line shows a projection of such a pyramid into the k_z plane.

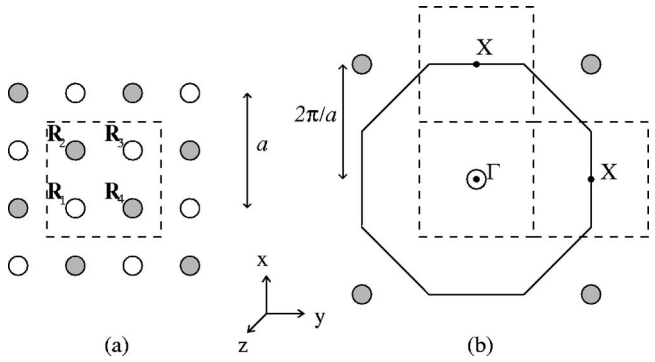

FIG. 2. (a) Cross section of a real-space tile (dashed line) for a $N_c=4$ cluster on the fcc lattice containing the points $\mathbf{R}_1=(0,0,0)$, $\mathbf{R}_2=(a/2,0,a/2)$, $\mathbf{R}_3=(a/2,a/2,0)$, and $\mathbf{R}_4=(0,a/2,a/2)$. The shaded sites lie outside of the page. (b) Cross section of the corresponding reciprocal-space tiles (dashed lines) for the $N_c=4$ cluster, with $\mathbf{K}_1=(0,0,0)$, $\mathbf{K}_2=(2\pi/a,0,0)$, and $\mathbf{K}_3=(0,2\pi/a,0)$ shown as the Γ point and the two X points. The fourth tile is centered at the X point $\mathbf{K}_4=(0,0,2\pi/a)$ and is situated out of the page vertically above Γ. Again the shaded points lie outside of the page and the solid line denotes a cross section of the first BZ in the (k_x,k_y) plane.

simple cubes of volume a^3 and $(2a)^3$, respectively, surrounding each cluster [see Fig. 1(c) for $N_c=2$].

(2) Label the sites of the original lattice by the set of vectors $\{\mathbf{R}_i^{orig}\}$, and the centers of the coarse-graining tiles by the set of vectors $\{\mathbf{R}_i^{cg}\}$.

(3) Label the reciprocal lattice corresponding to $\{\mathbf{R}_i^{orig}\}$ by the set of vectors $\{\mathbf{K}_i^{orig}\}$. Each $\mathbf{K}_i^{orig}$ is centered in a Brillouin zone Ω_{BZ} that periodically repeats to fill out all of reciprocal space. For the bcc lattice, this BZ will be a fcc Wigner-Seitz cell of volume $2(2\pi/a)^3$, as shown in Fig. 1(b).

(4) Label the reciprocal lattice corresponding to $\{\mathbf{R}_i^{cg}\}$ by the set of vectors $\{\mathbf{K}_i^{cg}\}$. Each $\mathbf{K}_i^{cg}$ is centered at a reciprocal space tile (corresponding to the reciprocal space of the real-space tile) that again periodically repeats to fill out all of reciprocal space. For the bcc lattice, $\{\mathbf{K}_i^{cg}\}$ are simple cubic and will be centered at simple cubic tiles of volume $(2\pi/a)^3$ or $(\pi/a)^3$ for the $N_c=2$ [see Fig. 1(d)] or $N_c=16$ cases, respectively.

(5) Observe that $\{\mathbf{K}_i^{orig}\}\subset\{\mathbf{K}_i^{cg}\}$. Select N_c vectors from the set $\{\mathbf{K}_i^{cg}\}$ that lie within Ω_{BZ} and do not differ by an element of $\{\mathbf{K}_i^{orig}\}$. We define these to be the set of cluster momenta $\{\mathbf{K}_n\}$. The reciprocal space contained within the N_c reciprocal-space tiles centered at $\{\mathbf{K}_n\}$ is completely equivalent to that contained within Ω_{BZ} by translation through reciprocal lattice vectors $\{\mathbf{K}_i^{orig}\}$. See Fig. 1(f) for the bcc example with $N_c=2$.

Refer to the table in Ref. 10 for the $\mathbf{R}_I$ and $\mathbf{K}_n$ values for sc, bcc, and fcc lattices obtained using the above method. Note that for the fcc lattice the next allowed cluster sizes are $N_c=4$ and 32, respectively, where the real-space tiles are again simple cubes of volume a^3 and $(2a)^3$, respectively, surrounding each cluster. See Fig. 2 for the fcc $N_c=4$ diagram.

Having carried out this coarse-graining procedure, we can now make an appropriate approximation to determine the effective medium. In reciprocal space, we approximate $\underline{\widehat{\delta G}}(\mathbf{k})$ within each of the N_c tiles by the N_c values $\{\underline{\widehat{\delta G}}(\mathbf{K}_n)\}$, each defined to be the average of $\underline{\widehat{\delta G}}(\mathbf{k})$ over the tile centered at $\mathbf{K}_n$. The scattering path matrix may then be represented by the set of coarse-grained values

$$\underline{\hat{\tau}}(\mathbf{K}_n)=\frac{N_c}{\Omega_{BZ}}\int_{\Omega_{\mathbf{K}_n}} d\mathbf{k}(\underline{\hat{t}}^{-1}-\underline{G}(\mathbf{k})-\underline{\widehat{\delta G}}(\mathbf{K}_n))^{-1}, \tag{4}$$

which are straightforward to calculate owing to $\underline{\widehat{\delta G}}(\mathbf{K}_n)$ being constant within each tile $\Omega_{\mathbf{K}_n}$. Note that the N_c integrals here have the same computational cost as one standard BZ integral. This is unlike a supercell method such as the MCPA where the size of the KKR matrix, which must be inverted at every $\mathbf{k}$ point, increases as N_c increases. In fact it is straightforward to show that this integration step is N_c times faster for the KKR-NLCPA than for a supercell method for comparable cluster sizes. Using Eq. (3), the scattering path matrix at the cluster sites becomes

$$\underline{\hat{\tau}}^{IJ}=\frac{1}{\Omega_{BZ}}\sum_{\mathbf{K}_n}\left(\int_{\Omega_{\mathbf{K}_n}} d\mathbf{k}(\underline{\hat{t}}^{-1}-\underline{G}(\mathbf{k})-\underline{\widehat{\delta G}}(\mathbf{K}_n))^{-1}\right)e^{i\mathbf{K}_n(\mathbf{R}_I-\mathbf{R}_J)}. \tag{5}$$

From Nyquist's sampling theorem,[29,30] the effect of coarse-graining the effective structure constant corrections is to reduce their range in real space. In fact from Eq. (3) we have

$$\underline{\widehat{\delta G}}(\mathbf{R}_{IJ})=\frac{1}{N_c}\sum_{\mathbf{K}_n}\underline{\widehat{\delta G}}(\mathbf{K}_n)e^{i\mathbf{K}_n(\mathbf{R}_I-\mathbf{R}_J)},$$

$$\underline{\widehat{\delta G}}(\mathbf{K}_n)=\sum_{J\neq I}\underline{\widehat{\delta G}}(\mathbf{R}_{IJ})e^{-i\mathbf{K}_n(\mathbf{R}_I-\mathbf{R}_J)}. \tag{6}$$

Note that $\underline{\widehat{\delta G}}(\mathbf{R}_{IJ})$ remains a translationally invariant quantity that depends only on the distance between sites I and J, now within the range of the cluster size, but independent of which site in the lattice is chosen to be site I.[9] It is now straightforward to generalize the CPA argument and determine the medium by mapping to an impurity cluster problem. We choose a real-space cluster consistent with the requirements outlined above, and use the embedded cluster method[15,16] to replace it with an "impurity" cluster of real t matrices and free-space structure constants in the (still undetermined) effective medium. We then consider all paths starting and ending on the impurity cluster sites and demand that the average over the 2^{N_c} possible impurity cluster configurations γ be equal to the path matrix for the effective medium itself, i.e.,

$$\sum_{\gamma} P_\gamma \underline{\tau}_\gamma^{IJ}=\underline{\hat{\tau}}^{IJ}, \tag{7}$$

where P_γ is the probability of configuration γ occurring. Therefore the effective medium t matrices and effective structure constant corrections are determined from a self-consistent solution of Eqs. (5) and (7). An example algorithm is given in Refs. 9 and 10. SRO may be included by appropriately weighting the configurations in Eq. (7) (the number of which can be reduced using symmetry and sampling),

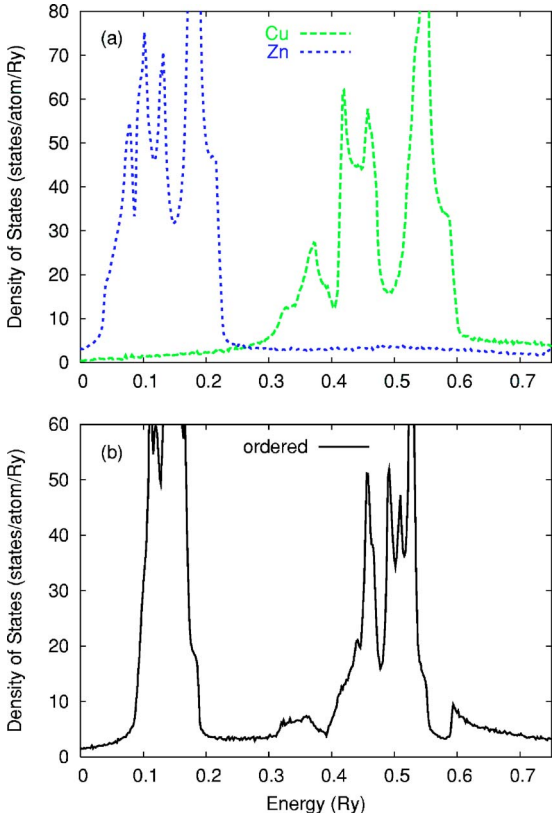

FIG. 3. (Color online) (a) DOS for pure Cu and pure Zn. (b) DOS for ordered $Cu_{50}Zn_{50}$.

provided that translational invariance is preserved. Observable quantities such as the density of states (DOS) can be calculated from the corresponding configurationally averaged Green's function.[31] The formula for the DOS within the KKR-NLCPA is given in Refs. 9 and 10. Importantly, owing to the translational invariance of the KKR-NLCPA medium, it is independent of lattice site chosen. This is crucial for calculating the partially averaged charge densities to be used in combination with DFT.[9,27,32–34] Finally, note that the KKR-NLCPA formalism reduces to the KKR-CPA for $N_c=1$, and nonlocal scattering correlations (and SRO if desired) are systematically included into the effective medium as N_c is increased, becoming exact as $N_c \to \infty$.

III. RESULTS

To illustrate the KKR-NLCPA, we present calculations for the bcc $Cu_{50}Zn_{50}$ solid solution with lattice constant 2.86 Å. In all calculations that follow, Cu and Zn potentials come from self-consistent field (SCF) KKR-CPA calculations,[35,36] the BZ integrals use the adaptive quadrature method,[37] and the energy contour has a 1-mRy imaginary part.

Figure 3(a) shows DOS plots for pure Cu and pure Zn, and Fig. 3(b) shows a calculation for the ordered $Cu_{50}Zn_{50}$ compound. Since the energies of the Cu and Zn d bands are very different, the system is said to be in the "split band" regime. Physically, this means an electron travels more easily between Cu or between Zn sites than between unlike sites

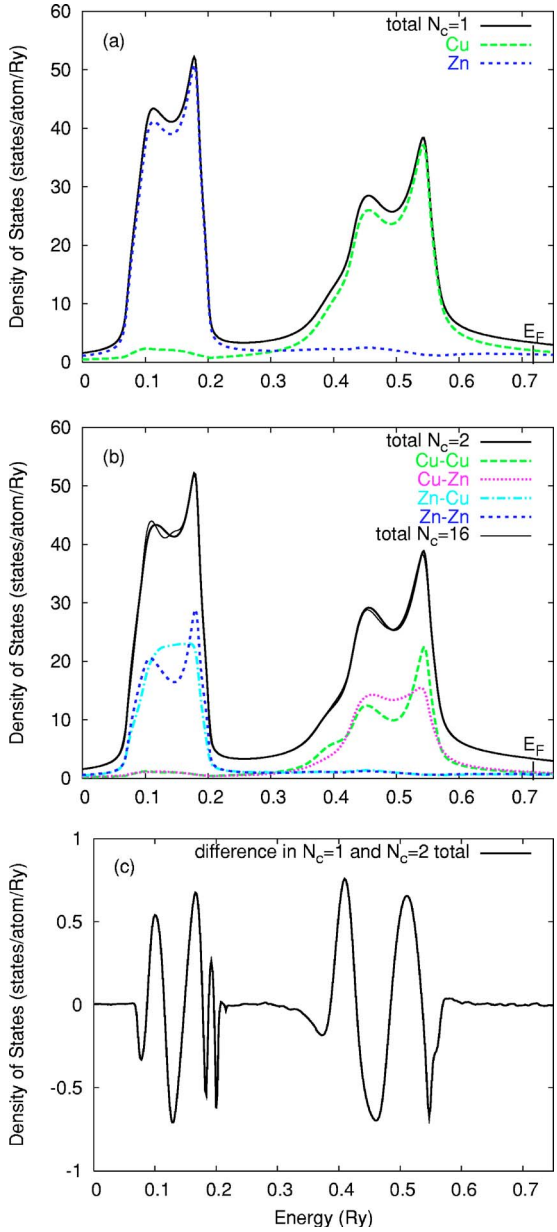

FIG. 4. (Color online) (a) Total average DOS for disordered bcc $Cu_{50}Zn_{50}$ using the KKR-CPA. Also shown are the contributions from the Cu and Zn components (site-restricted average DOS). E_F is the Fermi energy. (b) Total average DOS for bcc $Cu_{50}Zn_{50}$ using the KKR-NLCPA with $N_c=2$, along with the contributions from the four possible cluster configurations (cluster-restricted average DOS) measured at the first site, i.e., Cu for Cu-Cu, Cu-Zn, and Zn for Zn-Cu, Zn-Zn. (Owing to the translational invariance, contributions measured at the second site would give the same results with a simple reversal of the labels). Also shown are total DOS results for $N_c=16$. (c) Plot of the difference in the total DOS between the $N_c=1$ and 2 calculations, i.e., (total $N_c=1$) − (total $N_c=2$).

and so the decrease in overlap between like sites in the ordered case results in a narrowing of the Cu and Zn bands by a factor of 2 compared with the pure calculations.[38] Figure 4(a) shows KKR-CPA results for disordered $Cu_{50}Zn_{50}$. It is clear that the bands are widened and smoothened compared

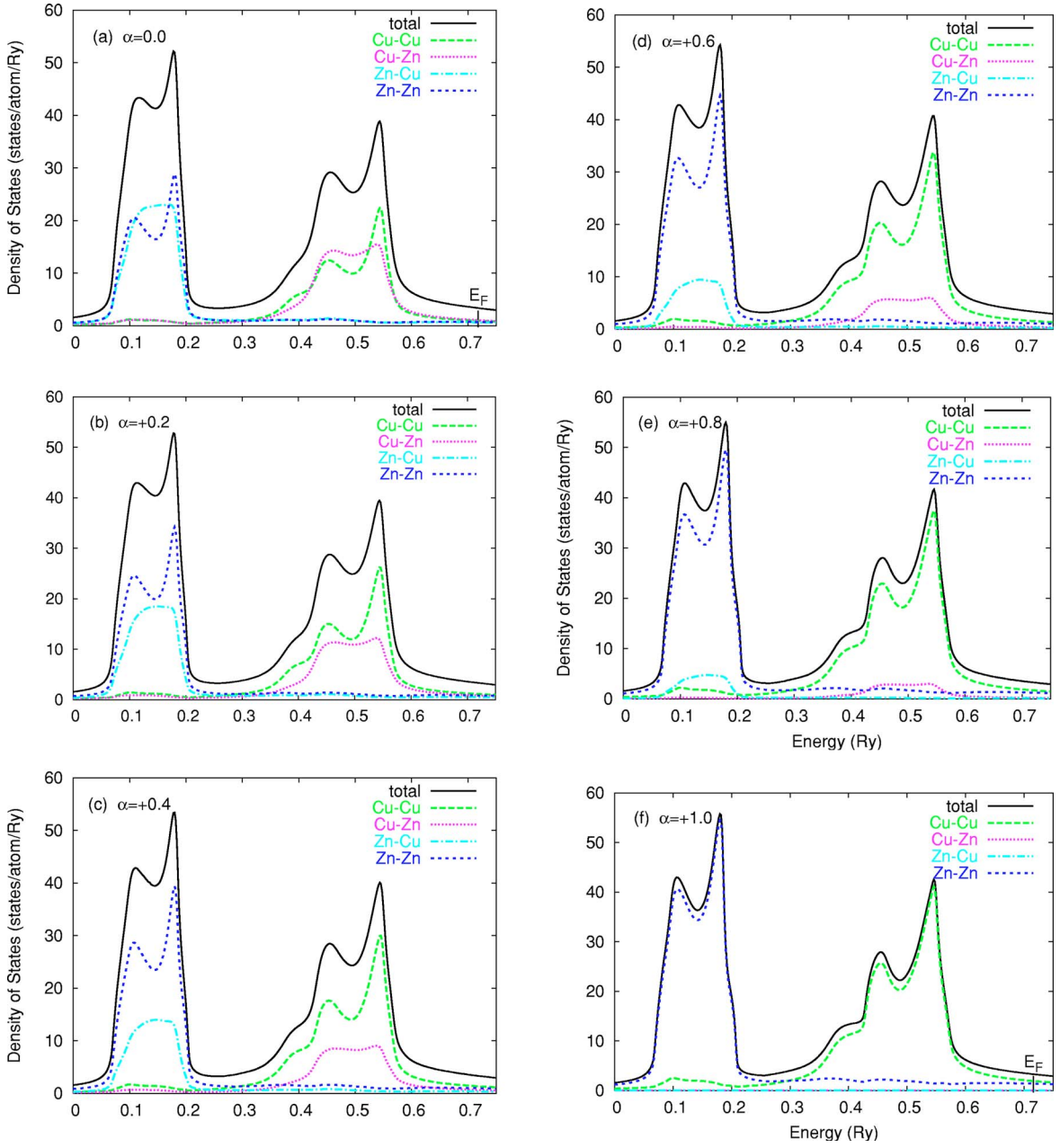

FIG. 5. (Color online) (a) Total and cluster component DOS for bcc $Cu_{50}Zn_{50}$ using the KKR-NLCPA with $N_c=2$ and $\alpha=0$. (b)–(f) Same as (a) but with increasing values of α, corresponding to short-range clustering.

with the DOS for the ordered calculation. The component contributions from Cu and Zn impurity sites embedded in the KKR-CPA medium are also shown. Next, a KKR-NLCPA calculation for disordered $Cu_{50}Zn_{50}$ for a two-site cluster ($N_c=2$) is shown in Fig. 4(b). First note that there is little observable difference in the total DOS compared with the KKR-CPA calculation. This is due to the small size of the cluster, and the difference due to the nonlocal scattering correlations shows up in detail only on a scale of ±1 state/atom/Ry, as shown in Fig. 4(c). As expected, it is clear that the extra structure is in the energy regions of the impurity d bands. However the most striking aspect of the KKR-NLCPA calculation is that the component contributions to the total DOS from the four possible cluster configurations are apparent. The component plots here are the DOS measured at the first cluster site when a particular cluster configuration is embedded in the KKR-NLCPA medium, which is the Cu site for the Cu-Cu and Cu-Zn configurations, and the Zn site for the Zn-Cu and Zn-Zn configurations. Crucially, owing to the translational invariance of the KKR-NLCPA medium, measurement at the second site gives the same results with a simple reversal of the labels of the Cu-Zn and Zn-Cu components. These component plots are particularly useful for interpreting the effects of SRO on the electronic structure, as described in the next section. Finally, Fig. 4(b) also shows total DOS results for the larger $N_c=16$ cluster, where the extra structure is more visible in the energy

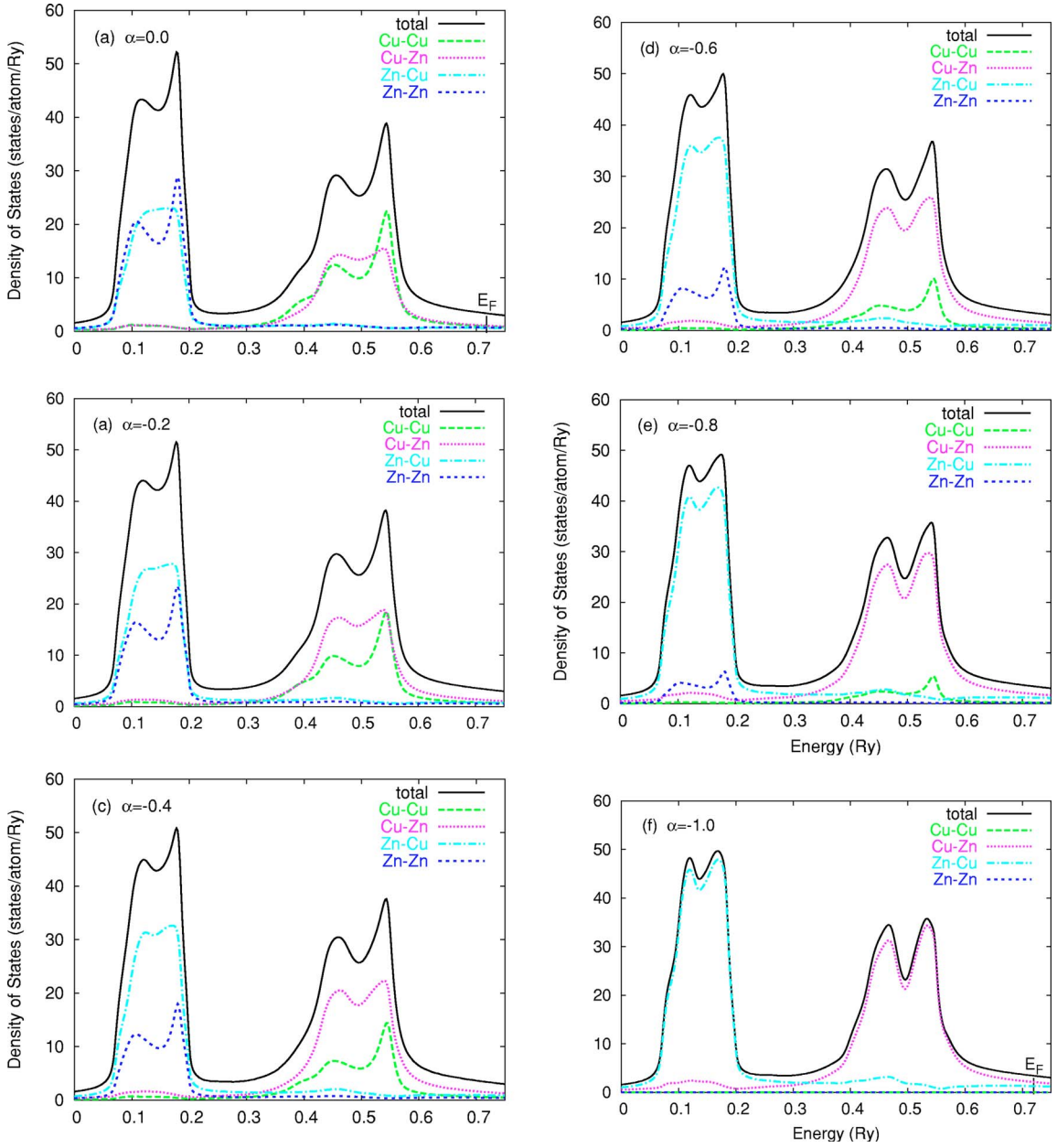

FIG. 6. (Color online) (a) Total and cluster component DOS for bcc $Cu_{50}Zn_{50}$ using the KKR-NLCPA with $N_c=2$ and $\alpha=0$. (b)–(f) Same as (a) but with decreasing values of α, corresponding to short-range ordering.

region between 0.10 and 0.15 Ry where some states are shifted to higher energies.

Short-range order

Unlike single-site theories, it is possible to include the effects of SRO on the electronic structure of disordered systems using the KKR-NLCPA. This may be done by using an appropriate nonrandom probability distribution when averaging over the impurity cluster configurations in Eq. (7). Of course, as the size of the cluster increases, the range of possible SRO that may be included also increases. Here we show results for bcc $Cu_{50}Zn_{50}$ using a pair cluster ($N_c=2$), where it is possible to include SRO between nearest-neighbor sites only. This may be straightforwardly done by introducing the nearest-neighbor Warren-Cowley SRO parameter α,[39] and using probabilities defined as

$$P(\mathrm{CuCu}) = P(\mathrm{Cu})^2 + \alpha/4,$$

$$P(\mathrm{ZnZn}) = P(\mathrm{Zn})^2 + \alpha/4,$$

$$P(\mathrm{CuZn}) = P(\mathrm{Cu})P(\mathrm{Zn}) - \alpha/4,$$

$$P(\mathrm{ZnCu}) = P(\mathrm{Zn})P(\mathrm{Cu}) - \alpha/4.$$

For $Cu_{50}Zn_{50}$, $P(\mathrm{Cu})=P(\mathrm{Zn})=0.5$ and so the SRO parameter can take values in the range $-1 \leqslant \alpha \leqslant 1$, where -1, 0, and

+1 correspond to ideal ordering, complete randomness, and ideal clustering.

Figure 5 shows the effects of short-range clustering upon the configurationally averaged DOS. It is clear that as α increases above zero, the probability of like pair components increases while that of unlike pairs decreases, resulting in corresponding changes to the component and total DOS. Indeed at $\alpha=+1$ the probability of unlike pairs is zero and the total DOS is now completely dominated by the features of the Cu-Cu and Zn-Zn components, as shown in Fig. 5(f). As expected, these features are reminiscent of the pure bands shown in Fig. 3(a), for example, the magnifying of the trough and peak on either side of 0.15 and 0.5 Ry can all be associated with the DOS for pure Zn and pure Cu, respectively. Moreover, a new peak appears just before 0.4 Ry associated with pure Cu. Figure 6 shows the effects of short-range ordering upon the configurationally averaged DOS. Here as α decreases below zero, the components of the total DOS due to like pairs decreases while that due to unlike pairs increases. Finally at $\alpha=-1$, as shown in Fig. 6(f), there are only contributions remaining from unlike pairs. Evidently, the DOS in general has a closer resemblance to that of ordered $Cu_{50}Zn_{50}$ shown in Fig. 3(b). For example, the peaks on either side of 0.15 and 0.5 Ry are now of roughly equal magnitude and there is also a slight overall narrowing of the bands compared with those for positive values of α due to the decrease in probability of like neighbors.

IV. CONCLUSIONS

The recently devised KKR-NLCPA generalizes the widely used KKR-CPA method by including SRO, and satisfies all of the requirements for a satisfactory effective-medium cluster theory.[16] It has relatively low computational cost in comparison with supercell-based methods since the BZ integration, the most computationally demanding aspect of a band-structure calculation, does not scale with the cluster size. In this paper we have implemented the KKR-NLCPA for a realistic system by illustrating the dramatic changes that can occur in the DOS for bcc $Cu_{50}Zn_{50}$.

Ultimately the KKR-NLCPA will be the electronic structure component of a fully self-consistent theory of disordered systems. The next step will be to combine it with DFT,[27] which will also enable charge correlations[32–34] and local lattice displacements[40] to be systematically taken into account for alloys. Then, the SRO parameter α will need to be coarse grained via Eqs. (6), and could be determined via a linear response calculation[41] before being fed back into the electronic structure, resulting in a completely *ab initio* theory of SRO at a given temperature T. Similar treatments will also be available for effects such as magnetic SRO in metallic magnets at finite temperature.

ACKNOWLEDGMENTS

Thanks to S. B. Dugdale and S. Ostanin for computational assistance. We acknowledge support from EPSRC (UK).

[1] B. L. Györffy, Phys. Rev. B **5**, 2382 (1972).
[2] G. M. Stocks, W. M. Temmerman, and B. L. Györffy, Phys. Rev. Lett. **41**, 339 (1978).
[3] B. L. Györffy, D. D. Johnson, F. J. Pinski, D. M. Nicholson, and G. M. Stocks in *Proceedings of the NATO Advanced Study Institute on Alloy Phase Stability*, edited by G. M. Stocks and A. Gonis (Kluwer, Dordrecht, 1987), p. 421.
[4] J. Kudrnovsky and V. Drchal, Phys. Rev. B **41**, 7515 (1990).
[5] J. B. Staunton and B. L. Györffy, Phys. Rev. Lett. **69**, 371 (1992).
[6] M. Lüders, A. Ernst, M. Dane, Z. Szotek, A. Svane, D. Koedderitzsch, W. Hergert, B. L. Györffy, and W. M. Temmerman, Phys. Rev. B **71**, 205109 (2005).
[7] J. S. Faulkner, Prog. Mater. Sci. **27**, 1 (1982).
[8] B. L. Györffy, B. Ginatempo, D. D. Johnson, D. M. Nicholson, F. J. Pinski, J. B. Staunton, and H. Winter, Philos. Trans. R. Soc. London, Ser. A **334**, 515 (1991).
[9] D. A. Rowlands, Ph.D. thesis, University of Warwick (2004).
[10] D. A. Rowlands, J. B. Staunton, and B. L. Györffy, Phys. Rev. B **67**, 115109 (2003).
[11] D. A. Rowlands, J. B. Staunton, B. L. Györffy, E. Bruno, and B. Ginatempo, cond-mat/0411347.
[12] H. Thomas, Z. Phys. **129**, 219 (1951).
[13] D. M. C. Nicholson and R. H. Brown, Phys. Rev. Lett. **70**, 3311 (1993).
[14] M. Tsukada, J. Phys. Soc. Jpn. **32**, 1475 (1972).
[15] A. Gonis, G. M. Stocks, W. H. Butler, and H. Winter, Phys. Rev. B **29**, 555 (1984).
[16] A. Gonis, *Green Functions for Ordered and Disordered Systems*, Vol. 4 of Studies in Mathematical Physics (North-Holland, Amsterdam, 1992).
[17] R. Mills and P. Ratanavararaksa, Phys. Rev. B **18**, 5291 (1978).
[18] A. Mookerjee, J. Phys. C **17**, 1511 (1987).
[19] S. S. A. Razee, S. S. Rajput, R. Prasad, and A. Mookerjee, Phys. Rev. B **42**, 9391 (1990).
[20] A. Mookerjee, J. Phys. C **6**, 1340 (1973).
[21] L. J. Kaplan and T. Gray, Phys. Rev. B **14**, 3462 (1976).
[22] S. S. Rajput, S. S. A. Razee, R. Prasad, and A. Mookerjee, J. Phys.: Condens. Matter **2**, 2653 (1990).
[23] A. Mookerjee and R. Prasad, Phys. Rev. B **48**, 17724 (1993).
[24] R. Haydock, V. Heine, and M. Kelly, J. Phys. C **5**, 2845 (1972).
[25] T. Saha, I. Dasgupta, and A. Mookerjee, Phys. Rev. B **50**, 13267 (1994).
[26] T. Saha, I. Dasgupta, and A. Mookerjee, J. Phys.: Condens. Matter **8**, 1979 (1996).
[27] D. A. Rowlands, J. B. Staunton, B. L. Györffy, E. Bruno, and B. Ginatempo (unpublished).
[28] M. H. Hettler, A. N. Tahvildar-Zadeh, M. Jarrell, T. Pruschke, and H. R. Krishnamurthy, Phys. Rev. B **58**, R7475 (1998).
[29] M. Jarrell and H. R. Krishnamurthy, Phys. Rev. B **63**, 125102 (2001).
[30] D. F. Elliot and K. R. Rao, *Fast Transforms: Algorithms, Analyses, Applications* (Academic, New York, 1982).
[31] J. S. Faulkner and G. M. Stocks, Phys. Rev. B **21**, 3222 (1980).
[32] E. Bruno, L. Zingales, and Y. Wang, Phys. Rev. Lett. **91**, 166401

(2003).
[33] J. S. Faulkner, Y. Wang, and G. M. Stocks, Phys. Rev. B **52**, 17106 (1995).
[34] J. S. Faulkner, Y. Wang, and G. M. Stocks, Phys. Rev. B **55**, 7492 (1997).
[35] G. M. Stocks and H. Winter, Z. Phys. B: Condens. Matter **46**, 95 (1982).
[36] D. D. Johnson, D. M. Nicholson, F. J. Pinski, B. L. Gyorffy, and G. M. Stocks, Phys. Rev. Lett. **56**, 2088 (1986).
[37] E. Bruno and B. Ginatempo, Phys. Rev. B **55**, 12946 (1997).
[38] V. L. Moruzzi, A. R. Williams, J. F. Janak, and C. Sofes, Phys. Rev. B **9**, 3316 (1974).
[39] J. M. Cowley, J. Appl. Phys. **21**, 24 (1950).
[40] N. Stefanou, P. J. Braspenning, R. Zeller, and P. H. Dederichs, Phys. Rev. B **36**, 6372 (1987).
[41] J. B. Staunton, D. D. Johnson, and F. J. Pinski, Phys. Rev. B **50**, 1450 (1994).